SCIENTIFIC REPORTS

OPEN

SUBJECT AREAS:
COORDINATION POLYMERS
BIOMEDICAL MATERIALS

Received
27 October 2014

Accepted
3 December 2014

Published
5 January 2015

Correspondence and requests for materials should be addressed to L.L. (liulibing@iccas.ac.cn) or S.W. (wangshu@iccas.ac.cn)

Synthesis and Characterization of Water-Soluble Polythiophene Derivatives for Cell Imaging

Fengyan Wang, Meng Li, Bing Wang, Jiangyan Zhang, Yongqiang Cheng, Libing Liu, Fengting Lv & Shu Wang

Beijing National Laboratory for Molecular Sciences, Key Laboratory of Organic Solids, Institute of Chemistry, Chinese Academy of Sciences, Beijing 100190, P. R. China.

In this work, four water-soluble polythiophene derivatives (PT, PT-DDA, PT-ADA, and PT-ADA-PPR) with different pendant moieties were synthesized via oxidative copolymerization by $FeCl_3$. By increasing the hydrophobic ability of side chain moieties, there is a gradually blue shift for the maximum absorption wavelength and red shift for the maximum emission wavelength, a reducing trend for fluorescence quantum yields, a growing trend for Stokes shift, and an increasing trend for the mean sizes in the order of PT, PT-ADA, and PT-DDA. All the synthesized polymers show low toxicity and good photostability and accumulate in the lysosomes of A549 cells. Furthermore, the introduction of porphyrin group to PT-ADA side chain (PT-ADA-PPR) broadens the absorption and emission ranges of PT-ADA. PT-ADA-PPR could be excited at two different excitation wavelengths (488 nm and 559 nm) and exhibits two emission pathways, and dual-color fluorescence images (orange and red) of PT-ADA-PPR accumulated in A549 cells are observed. Thus, PT-ADA-PPR could be used as an excellent dual-color fluorescent and lysosome-specific imaging material.

Fluorescent materials with high selectivity and sensitivity play an essential role not only in fundamental biology and pathophysiology but also in clinical diagnosis and therapy[1–3]. Organic dyes[1,4,5], fluorescent proteins[2,6,7], and quantum dots[3,8,9] have been intensively applied for the sensing and imaging of biological targets. However, rapid photobleaching of organic dyes and fluorescent proteins[10,11] and severe heavy-metal core-related cytotoxicity of quantum dots[12,13] stimulate the unremitting pursuit of developing new fluorescent materials.

Conjugated polymers (CPs), characterized by π-electron delocalized backbones, have been extensively tested in optoelectronic devices such as organic field-effect transistors[14,15], organic solar cells[16,17], and organic light-emitting diodes[18,19]. Water solubility of CPs could be acquired by introducing a charged group in the side chain of the polymer. These water soluble conjugated polymers (WSCPs) provide a versatile platform for highly sensitive chemical and biological sensing due to the unique light-harvesting ability and the signal amplification effect[20–23]. In addition, the WSCPs possess high fluorescence brightness and excellent photostability, thus they have been widely used in live cell imaging[24–27]. Among these WSCPs, water-soluble polythiophene derivatives (WSPTs) play an important role on live cell imaging because of their low cytotoxicity[27–29].

A lot of synthetic methods have been used to synthesize polythiophene derivatives (PTs), for example, nickel-mediated cross-coupling reactions[30], palladium-catalyzed cross-coupling reactions[29], oxidative polymerization[31], electrochemical polymerization[32], and biocatalyzed polymerization[33]. Oxidative polymerization catalyzed by $FeCl_3$ is one of the favored methods among the aforementioned synthetic methods to afford WSPTs because of the ease of this reaction. In fact, WSPTs synthesized using such method have been studied extensively for biological applications[31,34,35]. WSPTs with novel properties could be achieved by facile polymerization of functionalized thiophene monomers or simple modification with active substituents on the side chains of the polymers. For example, Wang and coworkers synthesized a water soluble polythiophene derivative with tyrosine kinase inhibitor lapatinib as pendant moieties, which was successfully applied for cell membrane imaging of living cells[27]. In order to develop water-soluble polythiophene derivatives (WSPTs) with new imaging functionality, herein, we synthesized a series of WSPTs (PT, PT-DDA, PT-ADA, and PT-ADA-PPR) via $FeCl_3$ oxidative copolymerization method. By varying hydrophobic moieties of side chains, their photophysical properties and mean sizes are tuned and exhibit certain rules. All of them show low toxicity and good photostability, and could

accumulate in the lysosomes of living A549 cells. Furthermore, the introduction of porphyrin group to PT-ADA side chain (PT-ADA-PPR) broadens the absorption and emission ranges of PT-ADA. PT-ADA-PPR could be excited at two different excitation wavelengths (488 nm and 559 nm) and exhibits two emission pathways. Subsequently, PT-ADA-PPR could be used as an effective dual-color lysosome-specific imaging agent.

Methods

Materials and Instruments. All chemicals were purchased from Acros, Aldrich Chemical Company or Alfa-Aesar and used as received. All organic solvents were purchased from Beijing Chemical Works and used as received. Compound **1**, **7** and **8** were synthesized according to procedures reported in the literatures[35–38]. **PT** was synthesized using previously reported procedures[36] and a further anion exchange procedure. A549 cell lines were purchased from Cell Culture Center of Institute of Basic Medical Sciences, Chinese Academy of Medical Sciences (Beijing, China). Fetal bovine serum (FBS) was obtained from Sijiqing Biological Engineering Materials (Hangzhou, China). Dulbecco's modified Eagle medium (DMEM) were purchased from HyClone/Thermofisher. Methylthiazolyldiphenyl-tetrazolium bromide (MTT) was obtained from Xinjingke Biotechnology Co., Ltd (Beijing, China). Hoechst 33342 and Lyso Tracker Blue DND-22 were purchased from Invitrogen. Fluorescence quantum yields (QYs) were measured with fluorescein (QY = 0.79) as the standard. The ^{1}H NMR and ^{13}C NMR spectra were recorded on Bruker Avance 300 MHz or 400 MHz or 500 MHz spectrometer. Mass spectra were recorded on a SHIMADZU LCMS-2010 spectrometer for ESI and a Waters GCT spectrometer for high resolution mass spectra (HRMS). Elemental analysis was measured on Flash EA1112. UV-Vis absorption spectra were obtained on a JASCOV-550 spectrophotometer. Fluorescence spectra were supplied by a Hitachi F-4500 fluorimeter equipped with a xenon lamp excitation source. In vitro cell viability assay was performed on a microplate reader (BIO-TEK Synergy HT, USA) at a wavelength of 490 nm. Photostability were measured with fluorescence microscopy (Olympus IX71) with a mercury lamp (100 W) as the light source. Confocal laser scanning microscopy (CLSM) characterization was conducted with a confocal laser scanning biological microscope (FV1000-IX81, Olympus, Japan).

Synthesis of N-(2-(2-(2-(2-(thiophen-3-yl)ethoxy)ethoxy)ethoxy)ethyl)dodecan-1-amine (2). Under nitrogen atmosphere, anhydrous potassium carbonate (33 mg, 0.24 mmol) was added into a solution of dodecylamine (111 mg, 0.60 mmol) in anhydrous ethanol (4 mL). The mixture was gradually heated up to 80°C, and then compound **1** (48 mg, 0.12 mmol) dissolved in anhydrous ethanol (1 mL) was added drop-wisely to the reaction mixture within an hour. The reaction mixture was refluxed under this condition over night. The resulting mixture was centrifuged. The supernatant was collected and then concentrated under vacuum. The residue was purified by silica gel chromatography using dichloromethane/methanol (v/v 50 : 1) as the eluent to afford a yellow-brown oil (25 mg, 50%). ^{1}H NMR (400 MHz, $CDCl_3$, δ): 7.23 (dd, 1H), 7.02 (d, 1H), 6.96 (d, 1H), 3.58–3.70 (m, 12H), 2.92 (t, 2H), 2.78 (t, 2H), 2.59 (t, 2H), 1.86 (s, 1H), 1.48 (t, 2H), 1.20–1.35 (br, 18H), 0.87 (t, 3H). ^{13}C NMR (400 MHz, $CDCl_3$, δ): 139.15, 128.46, 125.13, 121.09, 71.47, 70.54, 70.51, 70.41, 70.33, 70.21, 49.94, 49.23, 31.88, 30.62, 29.95, 29.64, 29.60, 29.55, 29.32, 27.35, 22.65, 14.09. HRMS (ESI) *m/z*: $[M + H]^+$ calcd. 428.3193; found 428.3188.

Synthesis of 3-(2-(2-(2-(2-azidoethoxy)ethoxy)ethoxy)ethyl)thiophene (3). To a solution of compound **1** (1.89 g, 4.56 mmol) in DMSO (40 mL) was added NaN_3 (0.62 g, 9.54 mmol) under nitrogen atmosphere. The mixture was heated to 70°C and stirred for 12 h, then was poured into 50 mL of water and extracted with CH_2Cl_2 for three times. The combined organic layer was dried over anhydrous Na_2SO_4 and concentrated under vacuum. The residue was purified by silica gel column chromatography using petroleum ether/ethyl acetate (v/v 4 : 1) as the eluent to afford a pale-yellow oil (1.24 g, 95%). ^{1}H NMR (400 MHz, $CDCl_3$, δ): 7.23 (dd, 1H), 7.03 (d, 1H), 6.98 (d, 1H), 3.60–3.75 (m, 12H), 3.38 (t, 2H), 2.93(t, 2H). ^{13}C NMR (400 MHz, $CDCl_3$, δ): 139.42, 128.73, 125.38, 121.35, 71.69, 71.06, 70.94, 70.90, 70.46, 70.26, 50.89, 30.86. ESI-MS *m/z*: $[M + Na]^+$ calcd. 308.1; found 308.2. $C_{12}H_{19}N_3O_3S$: calcd. C 50.51, H 6.71, N 14.73; found C 50.84, H 6.58, N 14.58.

Synthesis of tert-butyl (2-(2-(2-(2-(thiophen-3-yl)ethoxy)ethoxy)ethoxy) ethyl)carbamate (4). Triphenylphosphine (1.20 g, 4.58 mmol) was added into a solution of compound **3** (1.00 g, 3.50 mmol) in THF/H_2O (v/v 6 : 1, 40 mL). The mixture was stirred at room temperature for 12 h. Then, di-tert-butyl dicarbonate (1.52 g, 6.99 mmol) was added into the reaction mixture and continued stirring for 24 h. The reaction mixture was concentrated under vacuum and the resulting residue was purified by silica gel column chromatography using petroleum ether/ethyl acetate (v/v 3 : 1) as the eluent to afford a pale-yellow oil (1.16 g, 92%). ^{1}H NMR (400 MHz, $CDCl_3$, δ) 7.23 (dd, 1H), 7.02 (d, 1H), 6.96 (d, 1H), 5.02 (s, 1H), 3.69 (t, 2H), 3.57–3.66 (m, 8H), 3.53 (t, 2H), 3.25–3.37 (m, 2H), 2.92 (t, 2H), 1.43 (s, 9H). ^{13}C NMR (400 MHz, $CDCl_3$, δ): 156.19, 139.38, 128.69, 125.38, 121.33, 79.35, 71.70, 70.93, 70.81, 70.77, 70.46, 40.58, 30.84, 28.64. ESI-MS *m/z*: $[M + Na]^+$ calcd. 382.2; found 382.2. $C_{17}H_{29}NO_5S$: calcd. C 56.80, H 8.13, N 3.90; found C 57.10, H 8.10, N 3.87.

Synthesis of 2-(2-(2-(2-(thiophen-3-yl)ethoxy)ethoxy)ethoxy)ethanamine (5). A solution of compound **4** (568 mg, 1.58 mmol) in dichloromethane (10 mL) was purged with hydrogen chloride at room temperature. TLC was used to monitor the reaction process until the reactant was exhausted. The resulting mixture was concentrated under vacuum to give a pale-yellow solid. The obtained solid was dissolved in 5 mL of methanol, and then sodium hydroxide (748 mg, 18.70 mmol) dissolved in methanol solution (10 mL) was added. The reaction mixture was stirred at room temperature for 9 h, and the solvent was evaporated under reduced pressure. The residue was dissolved in 10 mL water and extracted with CH_2Cl_2 for three times. The organic layer was combined, washed with saturated sodium chloride solution and water, dried over anhydrous Na_2SO_4, and filtered. The solvent was removed to afford a yellow-brown oil (353 mg, 87%). ^{1}H NMR (400 MHz, $CDCl_3$, δ): 7.22 (dd, 1H), 7.01 (d, 1H), 6.95 (d, 1H), 3.58–3.72 (m, 10H), 3.49 (t, 2H), 2.91 (t, 2H), 2.84 (t, 2H), 1.33 (s, 2H). ^{13}C NMR (400 MHz, $CDCl_3$, δ): 139.25, 128.58, 125.24, 121.21, 73.55, 71.55, 70.68, 70.39, 70.32, 41.88, 30.71. HRMS (SIMS) *m/z*: $[M + H]^+$ calcd. 260.1315; found 260.1314.

Synthesis of N-(2-(2-(2-(2-(thiophen-3-yl)ethoxy)ethoxy)ethoxy)ethyl) adamantine-1-carbox- amide (6). To 5 mL of dichloromethane, compound **5** (100 mg, 0.39 mmol) and anhydrous triethylamine (43.8 mg, 0.43 mmol) were added and the mixture was kept at 0 °C. Adamantane chloride (85 mg, 0.428 mmol) dissolved in CH_2Cl_2 (1 mL) was added drop by drop to the reaction mixture. Then the mixture was slowly warmed to room temperature and stirred for 35 h. The reaction was quenched with water and extracted with CH_2Cl_2 for three times. The combined organic layer was dried over anhydrous Na_2SO_4, filtered and concentrated under vacuum. The crude product was purified by silica gel column chromatography using petroleum ether/ethyl acetate (v/v 2 : 3) as the eluent to afford a yellow-brown oil (110 mg, 67%). ^{1}H NMR (400 MHz, $CDCl_3$, δ): 7.23 (dd, 1H), 7.01 (d, 1H), 6.96 (d, 1H), 6.11 (s, 1H), 3.55–3.72 (m, 10H), 3.52 (t, 2H), 3.42 (dd, 2H), 2.91 (t, 2H), 2.01 (br, 3H), 1.83 (d, 6H), 1.62–1.78 (m, 6H). ^{13}C NMR (400 MHz, $CDCl_3$, δ): 178.11, 139.21, 128.55, 125.30, 121.24, 71.61, 70.65, 70.61, 70.35, 70.04, 40.68, 39.28, 39.06, 36.64, 30.72, 28.25. HRMS (SIMS) *m/z*: $[M + H]^+$ calcd. 422.2360; found 422.2360.

Synthesis of PPR. Anhydrous potassium carbonate (56 mg, 0.41 mmol) was added into a mixed solution of compound **1** (60 mg, 0.14 mmol) and compound **7** (100 mg, 0.15 mmol) in DMF (3 mL). Then the mixture was heated to 70 °C and stirred for 24 h. A diaphragm pump was used to remove DMF when the reaction was completed. The resulting crude product was purified by silica gel column chromatography using chloroform as the eluent to give **PPR** (110 mg, 88%) as a purple solid. ^{1}H NMR (400 MHz, $CDCl_3$, δ): 8.84 (s, 8H), 8.06–8.09 (m, 8H), 7.51 (d, 6H), 7.19–7.23 (m, 3H), 7.01 (d, 1H), 6.96 (d, 1H), 4.31 (t, 2H), 3.97 (t, 2H), 3.80 (t, 2H), 3.64–3.74 (m, 8H), 2.93 (t, 2H), 2.67 (s, 9H), −2.75 (s, 2H). ^{13}C NMR (400 MHz, $CDCl_3$, δ): 158.58, 139.30, 139.20, 137.29, 135.52, 134.79, 134.51, 128.52, 127.40, 125.18, 121.15, 120.10, 119.74, 112.80, 71.50, 70.96, 70.76, 70.70, 70.29, 69.89, 67.64, 30.67, 21.51. HRMS (SIMS) *m/z*: $[M + H]^+$ calcd. 915.3938; found 915.3932.

General procedure for oxidative polymerization. Compound **8** and the other required monomers (**2**, **6**, **PPR**) were dissolved in 15 mL $CHCl_3$. The resulting solution was stirred for 15 min under nitrogen atmosphere, then anhydrous $FeCl_3$ (4.5 equiv. of the total molar amount of the monomers) was added. The mixture was stirred for two days at the ambient temperature. After the solvent was removed gently, the residue was dissolved with methanol. Hydrazine hydrate (for PT-DDA) or saturated potassium carbonate (for PT-ADA and PT-ADA-PPR) was used to precipitate ferric chloride. The combined filtrate was evaporated under reduced pressure and the residue was dissolved in DMSO/H_2O (v/v 1:10). Then the solution was dialyzed through a membrane with a molecular weight cutoff of 3500 for three days and freeze-dried to yield a red sticky substance. The red sticky polymer was dissolved in a small quantity of methanol. Then, an excess of tetrabutylammonium chloride was added into the above solution. The resulting solution was added drop by drop to an excess of actone to afford a red precipitation. After centrifugation, the resulting polymer was washed several times with a saturated solution of tetrabutylammonium chloride in acetone. Excess tetrabutylammonium chloride was removed by Soxhlet extraction with acetone over a period of 6 h. The final polymer was dissolved in deionized water and freeze-dried to obtain a red sticky substance.

PT-DDA (Yield: 13%): ^{1}H NMR (400 MHz, d ^{6}-DMSO, δ): 7.30–7.51 (br, 2.00H), 3.81 (br, 6.03H), 3.48–3.70 (br, 18.15H), 3.22–3.48 (br, 70.89H), 3.00–3.20 (br, 22.79H), 2.72–2.86 (br, 2.09H), 1.51 (s, 1.00H), 1.23 (br, 3.81H), 0.88 (br, 1.74H).

PT-ADA (Yield: 30%): ^{1}H NMR (400 MHz, d ^{6}-DMSO, δ): 7.20–7.50 (br, 2.00H), 3.82 (br, 4.44H), 3.73 (br, 1.79H), 3.48–3.69 (br, 24.64H), 3.21–3.48 (br, 61.02H), 3.07–3.21 (br, 23.94H), 2.70–2.88 (br, 2.11H), 1.91 (br, 0.78H), 1.71 (br, 1.71H), 1.6 (br, 1.35H).

PT-ADA-PPR (Yield: 18%): ^{1}H NMR (400 MHz, d ^{6}-DMSO, δ): 8.83 (br, 8.00H), 8.09 (br, 6.93H), 7.54 (br, 7.92H), 7.22–7.45 (br, 12.61H), 4.39 (br, 3.17H), 4.10 (br, 2.25H), 3.80–4.02 (br, 11.79H), 3.72 (br, 8.27H), 3.45–3.69 (br, 81.78H), 3.25–3.69 (br, 57.16H), 2.92–3.25 (br, 72.19H), 2.84 (br, 10.06H), 2.67 (br, 12.66H), 1.90 (br, 9.26H), 1.71(br, 9.43H), 1.60 (br, 12.86H), −2.9 (br, 2.23H).

Assay for photostability of WSPTs. The solution of various WSPTs at the concentration of 1 mM in RU was dropped on a Fisherfinest Premium Superslip, and the sample was continuously irradiated by a mercury lamp (100 W) with a 450/

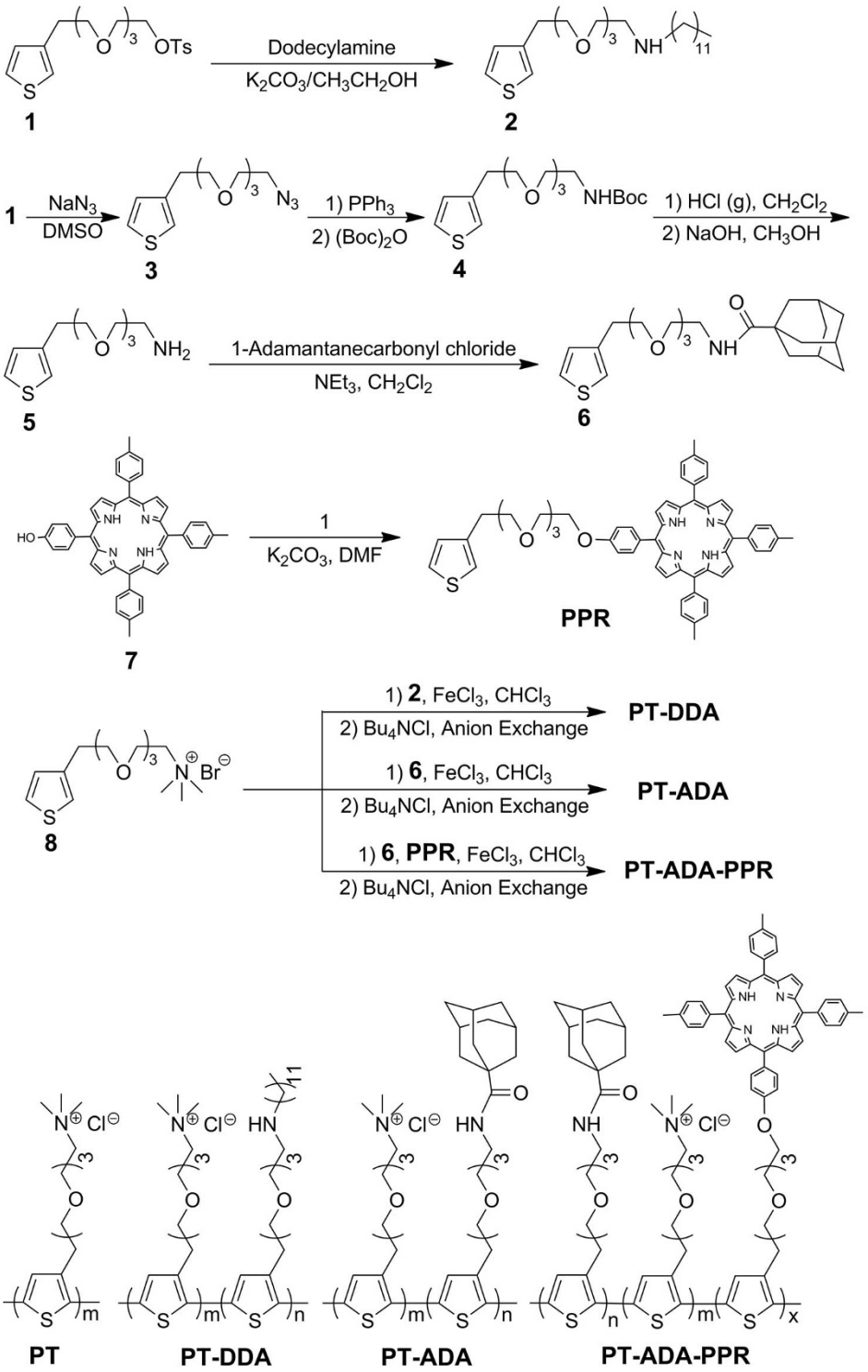

Figure 1 | Synthetic routes and chemical structures of the four WSPTs.

70 nm excitation filter. Fluorescence emission intensities of samples were recorded with fluorescence microscopy (Olympus IX71).

Cell culture. Human lung cancer (A549) cells were grown in DMEM with 10% FBS at 37 °C under a humidified atmosphere containing 5% CO_2. The cells were routinely passed by treatment with trypsin.

In vitro cell viability assay. A549 cells were seeded in 96-well culture plates at a density of 1×10^4 cells/well. After 20 h incubation, the culture medium were replaced by fresh culture medium with various concentrations of different WSPTs. Followed by 24 h incubation, MTT (5 mg·mL^{-1} in water, 10 μL/well) was added into each well. After incubation for 4 h at 37 °C, the supernatant was abandoned and 100 μL of DMSO was added into each well to dissolve the produced formazan. After shaking the plates for 5 min, absorbance values of the produced purple formazan were recorded with a microplate reader at 490 nm.

Cell imaging and localization. A549 cells were seeded in 35 mm Petri dish with a glass bottom at a density of approximately 10% per plate. After incubation at 37 °C for 12 h, the medium was replaced by fresh culture medium with various WSPTs (the final concentration was 20 μM in RU). The cells were further cultured for 24 h. Then the culture medium was abandoned and the cells were washed thrice with phosphate-buffered saline (PBS, pH = 7.4).

(1) For cell imaging: The cells were fixed at room temperature for 20 min using 4% paraformaldehyde and then washed thrice with PBS. Hoechst 33342 (the final concentration was 10 μg/mL) in PBS was added and incubated at room tem-

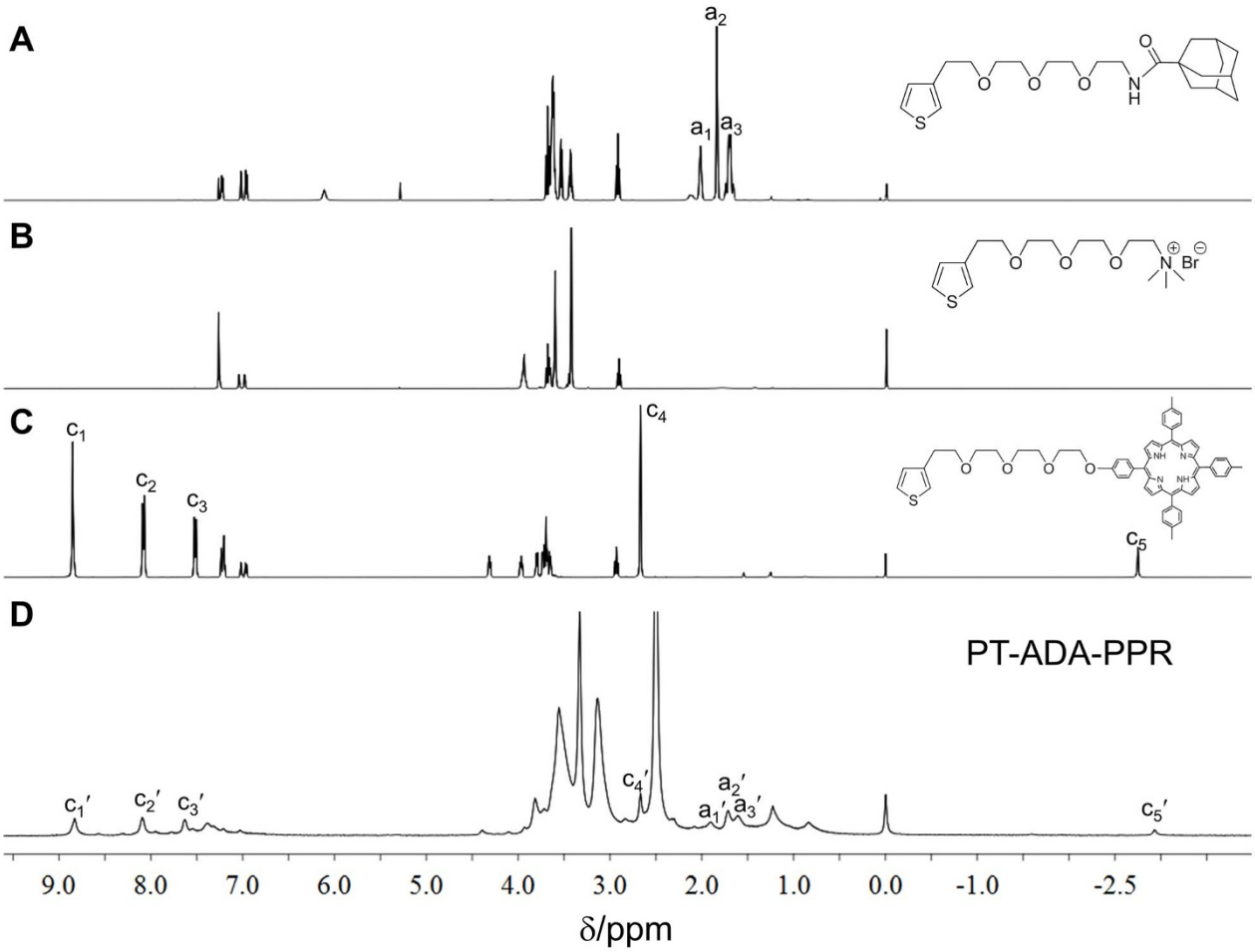

Figure 2 | ^{1}H NMR spectra of PT-ADA-PPR and the corresponding monomers. The solvent was $CDCl_3$ for (A), (B) and (C), and d ^{6}-DMSO for (D).

perature for 5 min. After washing thrice with PBS, the images of the cells were taken by confocal laser scanning microscopy (CLSM).

(2) For localization: Lyso Tracker Blue DND-22 (the final concentration was 0.5 μM) was added and allowed to incubate with A549 cells for 30 min. The cells were washed thrice with PBS, and their images were taken by CLSM.

(3) For dual-channel imaging: The above cells were directly used to take images by CLSM upon exciting at 488 nm and 559 nm.

Results and Discussion

The synthetic routes for all of the monomers and water-soluble polythiophene derivertives (WSPTs) are outlined in Figure 1. Substitute compound **1** with dodecylamine, NaN_3 or **7**, give compound **2**, **3** and **PPR** in 50%, 95% and 88% yields, respectively. Reduction of compound **3** by triphenylphosphine in THF/H_2O (v/v 6:1) and followed by protection of the obtained amino groups with di-tert-butyl dicarbonate gives compound **4** in a 92% yield. Deprotection of the tert-butoxycarbonyl group using hydrogen chloride and neutralization of the formed hydrochloride salt using a methanol solution of sodium hydroxide affords compound **5** in 87% yield. The condensation reaction of compound **5** and adamantane chloride in the presence of anhydrous triethylamine gives compound **6** in a 67% yield. Oxidative copolymerization of different monomers under nitrogen atmosphere in the presence of $FeCl_3$ and a subsequent anion exchange procedure[31] give PT-DDA, PT-ADA, and PT-ADA-PPR in 13%, 30%, and 18% yield, respectively. ^{1}H NMR spectroscopy was used to characterize the synthesized WSPTs and determine the actual ratio of the copolymerized monomers. Take the ^{1}H NMR spectra of PT-ADA-PPR and the corresponding monomers shown in Figure 2 as an example. The peaks marked with a_1-a_3 and c_1-c_5 are the characteristic peaks corresponding to the adamantane moiety of monomer **6** and the porphyrin moiety of **PPR**, respectively. Obviously, the peaks marked with a_1'-a_3' and c_1'-c_5' are separately corresponding

Table 1 | Composition, Optical Properties and Mean Sizes of the Four WSPTs

WSPTs	Feed Ratio (m : n : x)	Actual Ratio[a] (m : n : x)	$\lambda_{max,abs}$[b] (nm)	$\lambda_{max,em}$[b] (nm)	Stokes shift (nm)	QY[c] (%)	Mean sizes[b] (nm)
PT-ADA-PPR	7 : 2 : 1	72 : 17 : 11	424	573	149	2	85.2 ± 2.5
PT	1 : 0	100 : 0	410	565	155	10	104.9 ± 1.8
PT-ADA	9 : 1	81 : 19	400	571	171	9	152.4 ± 1.8
PT-DDA	9 : 1	88 : 12	394	575	181	6	161.5 ± 15.8

[a]Determined by ^{1}H NMR.
[b]Measured in aqueous solution with a concentration of 100 μM in RU.
[c]Measured in aqueous solution with fluorescein as standard.

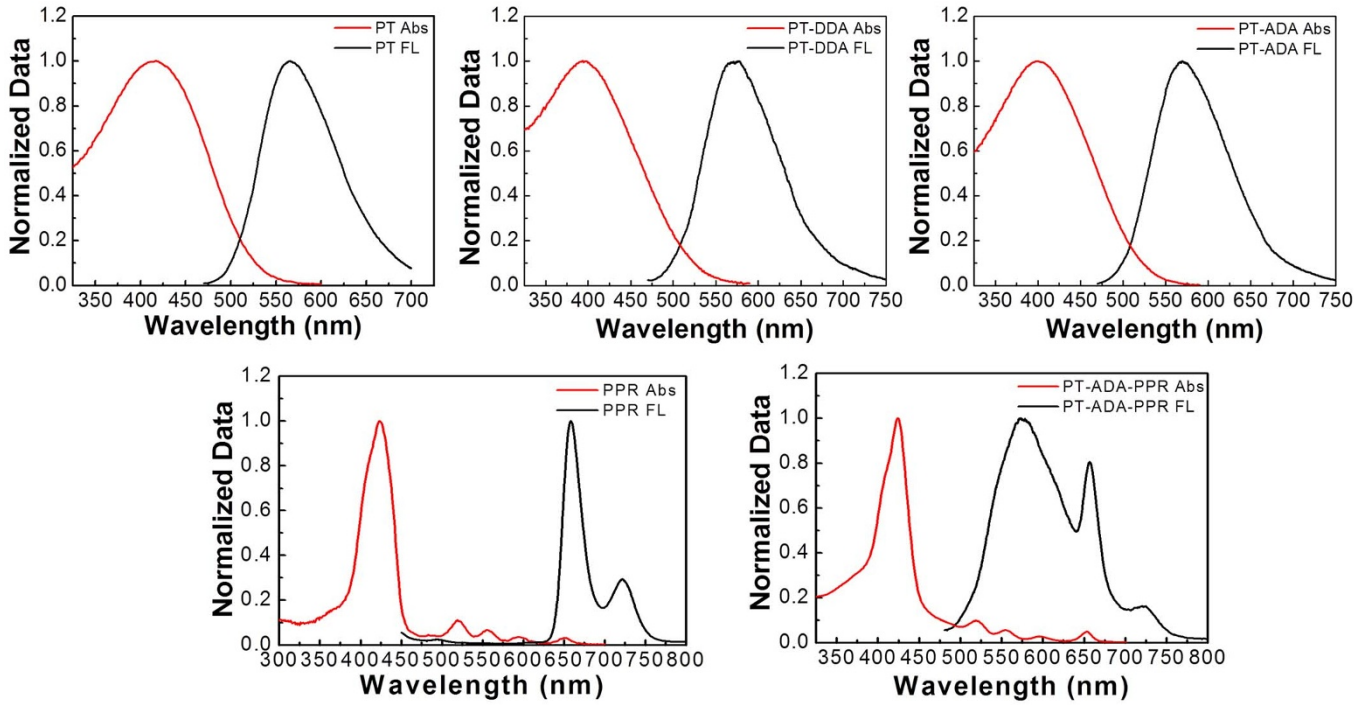

Figure 3 | Normalized UV-Vis absorption and fluorescent emission spectra of four WSPTs and monomer PPR. [WSPTs] = 100 μM in RU. [PPR] = 11 μM. The excitation wavelength is 460 nm for WSPTs, and 420 nm for PPR.

to that marked with a_1-a_3 and c_1-c_5. Thus, monomer **6** and **PPR** are successfully copolymerized with monomer **8** to construct PT-ADA-PPR. By calculating the proportion of the characteristic hydrogen in the ^{1}H NMR spectrum of PT-ADA-PPR, the actual ratio of monomer **8**, **6**, and **PPR** were determined to be 72%, 17%, and 11%, respectively. The spectra of PT-DDA, PT-ADA, and the corresponding monomers are shown in Figure S1 and analyzed using the way mentioned above, and the obtained actual ratio of the copolymerized monomers of them are summarized in Table 1.

All of the four WSPTs are soluble in water due to the dominant quaternized amine-terminated side chain. However, they exhibit different properties because of the introduction of different pendant

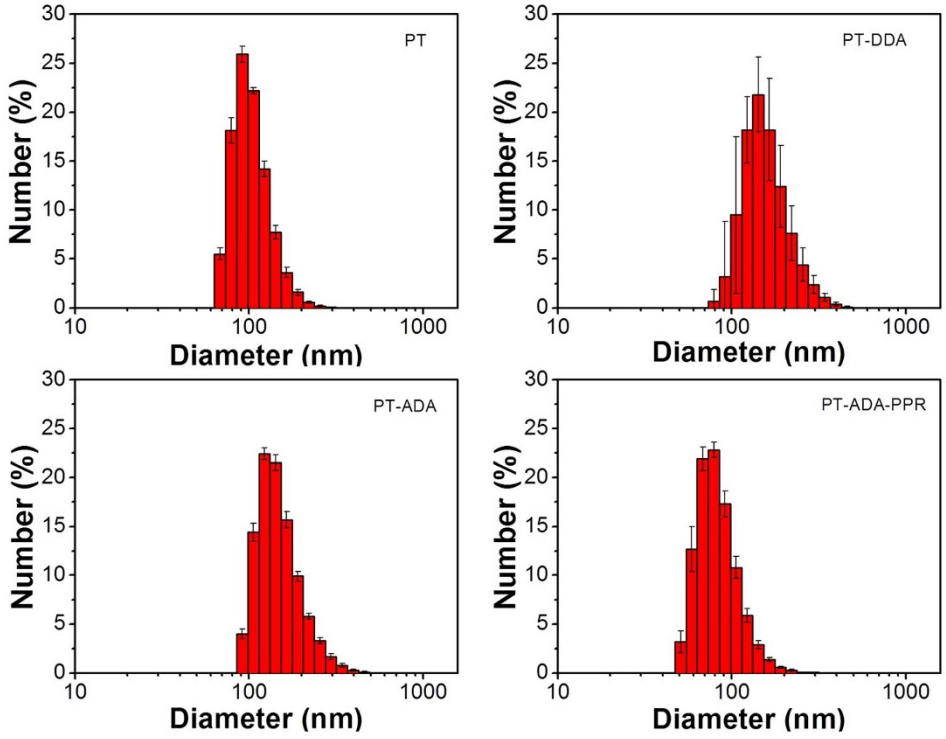

Figure 4 | Hydrodynamic diameter distribution of the four WSPTs (100 μM in RU) in water.

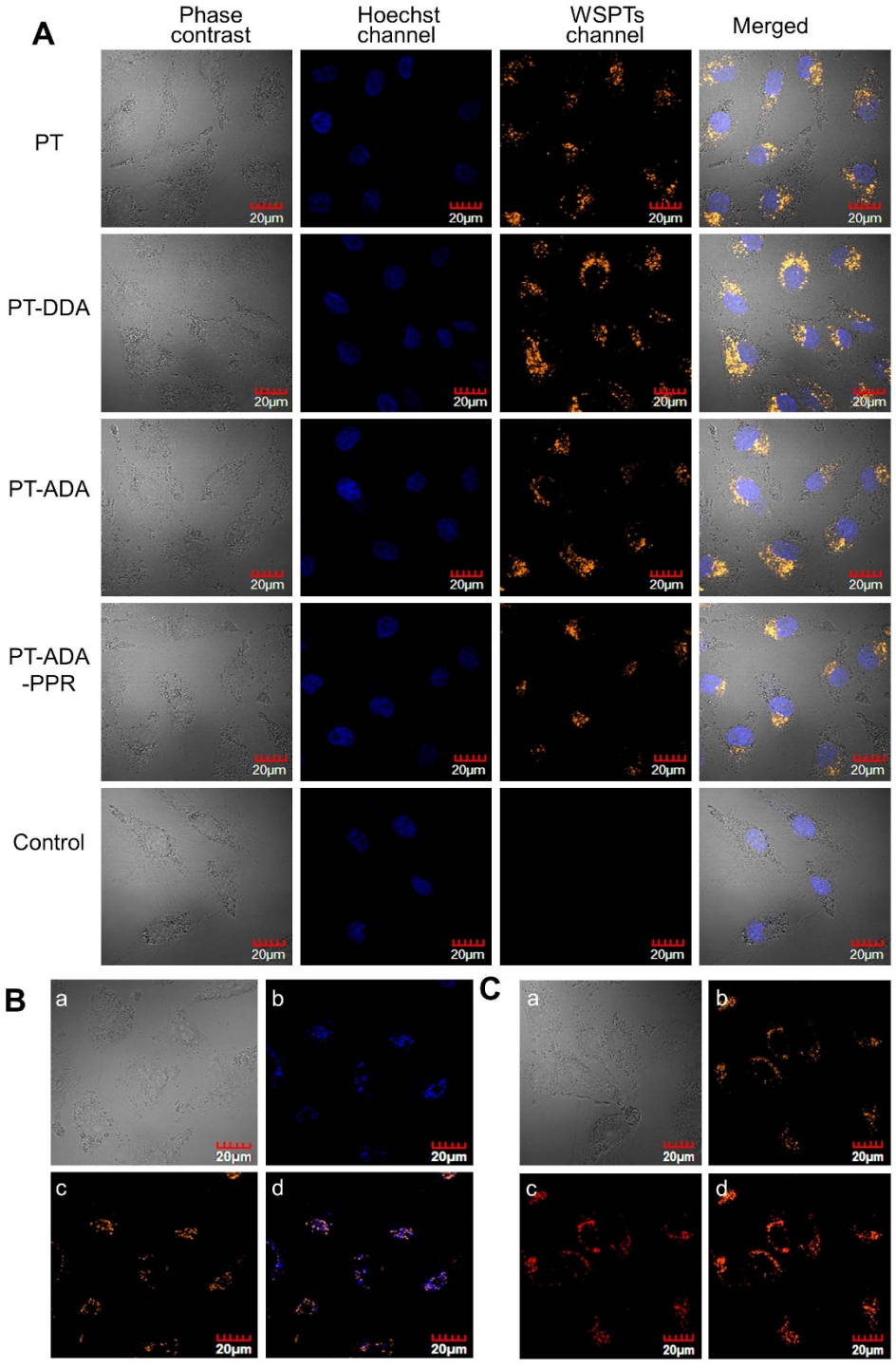

Figure 5 | (A) Cellular location of WSPTs after 24 h incubation with A549 cells. Hoechst 33342 (excitation: 405 nm; collection: 425 to 475 nm), WSPTs (excitation: 488 nm; collection: 540 to 640 nm). (B) Co-location imaging of PT and Lyso Tracker Blue DND-22 (0.5 μmol/L) in A549 cells. (a) phase contrast image; (b) fluorescence image of Lyso Tracker Blue DND-22 (excitation: 405 nm; collection: 415 to 460 nm); (c) fluorescence image of PT (excitation: 488 nm; collection: 540 to 640 nm); (d) overlapped image of (b) and (c). (C) Dual-channel fluorescence images of PT-ADA-PPR in A549 cells. (a) phase contrast image; (b) fluorescence image of the back bone of PT-ADA-PPR (excitation: 488 nm; collection: 500 to 600 nm); (c) fluorescence image of PPR (excitation: 559 nm; collection: 655 to 755 nm); (d) overlapped image of (b) and (c). The false color of Hoechst 33342 (nuclei stain), Lyso Tracker Blue DND-22 (lysosome stain), WSPTs and PPR is blue, blue, orange and red, respectively. [WSPTs] = 20 μM (in RU). [Hoechst 33342] = 10 μg/mL.

moieties. The photophysical properties (Figure 3) and sizes of the aggregates (Figure 4) of the four WSPTs were investigated in aqueous solution and summarized in Table 1. PT exhibits a maximum absorption at 410 nm, corresponding to the π–π* transition of the back bone. Its emission displays a maximum peak at 565 nm with a Stokes shift of 155 nm and a fluorescence quantum yield (QY) of 10%. The maximum absorption wavelength of PT-ADA is 400 nm and the emission maximum is 571 nm with a Stokes shift of 171 nm and a QY of 9%. To PT-DDA, the maximum absorption and emission wavelength is 394 nm and 575 nm, respectively, with a Stokes shift

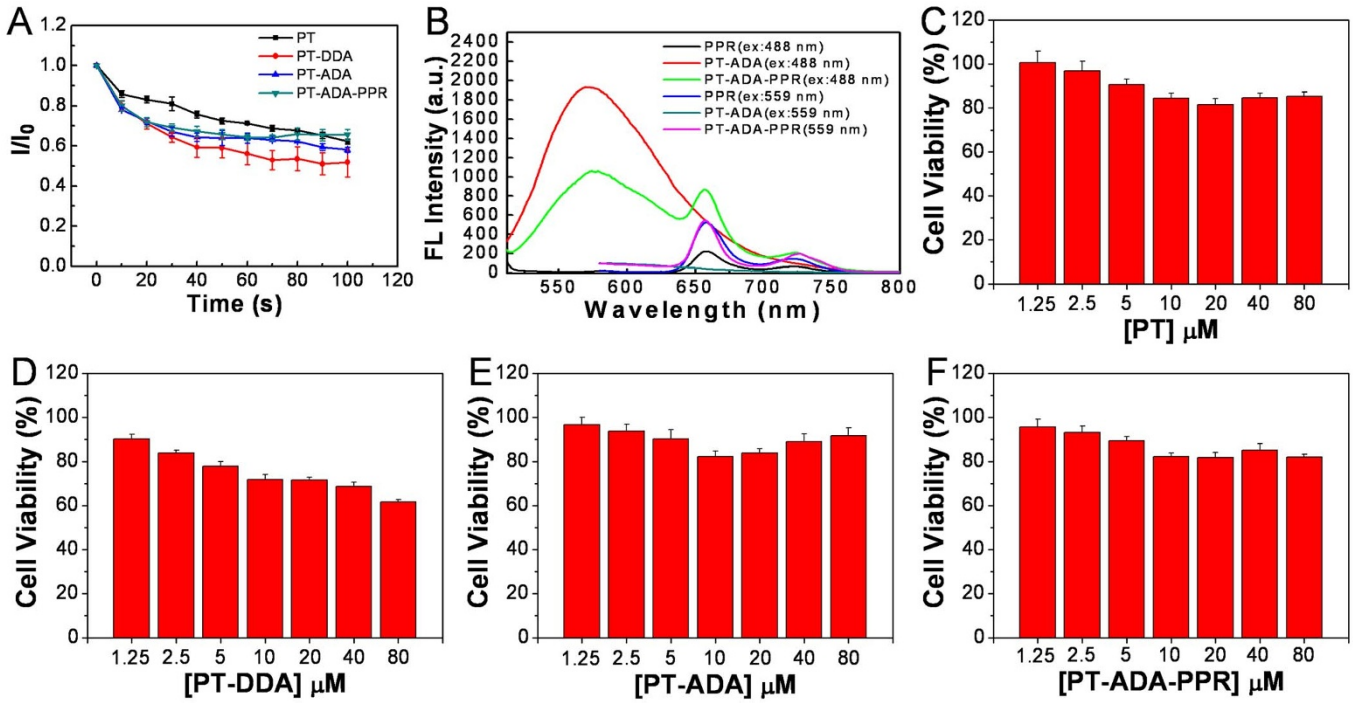

Figure 6 | (A) Photostability of the four WSPTs under a mercury lamp (100 W) irradiation with an excitation filter of 450/70 nm. (B) Fluorescent emission spectra of PPR, PT-ADA and PT-ADA-PPR excited at 488 nm and 559 nm. [WSPTs] = 10 μM (in RU); [PPR] = 1.1 μM. (C–F) Cell viability of A549 cells treated with the four WSPTs by using a typical MTT assay.

of 181 nm and a QY of 6%. The mean sizes are 104.9 ± 1.8 nm, 152.4 ± 1.8 nm, and 161.5 ± 15.8 nm for PT, PT-ADA, and PT-DDA, respectively. Thus, with increasing the hydrophobic ability of pendant moieties, there is a gradually blue shift for the maximum absorption wavelength and red shift for the maximum emission wavelength, a reducing trend for fluorescence quantum yields, a growing trend for Stokes shift, and an increasing trend for the mean sizes in the order of PT, PT-ADA, and PT-DDA. However, the optical properties and mean sizes of PT-ADA-PPR don't meet the aforementioned rules due to the introduction of the porphyrin moiety. For the case of PT-ADA-PPR, the maximum absorption and emission wavelength are 424 nm and 573 nm, respectively, with a Stokes shift of 149 nm and a QY of 2%. Compared with PT-ADA, both the maximum absorption and emission wavelength exhibit a red shift, and both the Stokes shift and QY decrease. Besides, the mean size of PT-ADA-PPR (85.2 ± 2.5 nm) is much smaller than that of PT-ADA. This phenomenon may be related to the stacking of the porphyrin group which makes PT-ADA-PPR aggregates more tightly[39].

These WSPTs were applied for in vitro cell imaging and localization. Confocal laser scanning microscopy images in Figure 5A show that all of the four WSPTs are accumulated in the cytoplasm, especially around the perinuclear region. To further identify their cellular location, the cells were co-stained with PT and a lysosome-specific dye (Lyso Tracker Blue DND-22) as shown in Figure 5B. The overlapped image of lysosome-specific dye (blue) and PT (orange) shows that PT mainly accumulates in the lysosomes of A549 cells. Moreover, the other three WSPTs also accumulate in the lysosomes of A549 cells (Figure S2). Photostability measurement (Figure 6A) shows that the fluorescence of WSPTs retains more than 50% of the original intensity after continuously irradiating at 455 nm for 100 s. In addition, the cytotoxicity of these WSPTs were assayed using the MTT method, a standard method in which the conversion of 3-(4,5-dimethylthiazol-2-yl)-2,5-diphenyl-2H-tetrazolium hydrobromide (MTT) to formazan is related to the cell viability[40]. More than 80% cell viabilities were obtained in the presence of an increasing concentration of WSPTs (from 1.25 μM to 80 μM) except PT-DDA (more than 60%) after 24 h incubation with A549 cells in dark (Figure 6C–F), which indicates that these WSPTs do not display obvious cytotoxicity. The results suggested that these WSPTs could be used as excellent lysosome-specific imaging materials because of the good photostability and low cytotoxicity.

To our surprise, the introduction of porphyrin group makes PT-ADA-PPR possess excellent photophysical properties. Compared with PT-ADA, the absorption spectrum of PT-ADA-PPR exhibits a sharp peak at 424 nm and four weak absorption peaks at 519 nm, 556 nm, 595 nm, and 654 nm, which corresponding to the Soret band and Q bands of PPR (Figure 3). The emission spectrum of PT-ADA-PPR shows two more emission peaks at 656 nm and 725 nm, which correspond to the emission of PPR (Figure 3). The introduction of the porphyrin group broadens both the absorption and emission ranges of WSPTs, which makes PT-ADA-PPR to possess potential usage in multicolor imaging. To confirm this speculation, PPR (1.1 μM), PT-ADA (10 μM in RU), and PT-ADA-PPR (10 μM in RU) were excited at both 488 nm and 559 nm. The results in Figure 6B show that the fluorescence intensities of PPR and PT-ADA-PPR have no obvious difference when excited at 559 nm. That is to say, the actual ratio of PPR determined by ^{1}H NMR is accurate to a certain extent. However, when excited at 488 nm, the fluorescence intensity of PT-ADA-PPR is much larger than that of PPR. Thus, efficient intramolecular fluorescence resonance energy transfer (FRET) occurs from the polymer backbone to the porphyrin moiety. In addition, PT-ADA-PPR could be excited at both 488 nm and 559 nm and exhibit two emission peaks between 630 nm and 800 nm, while PT-ADA cannot be excited at 559 nm and no emission peaks between 630 nm and 800 nm are observed. On the basis of the photophysical properties of PT-ADA-PPR, in vitro cell imaging experiments were conducted. Upon excitation at 488 nm (collection: from 500 to 600 nm) and 559 nm (collection: from 655 to 755 nm), dual-color fluorescence images (orange and red) of PT-ADA-PPR accumulated in A549 cells were obtained (Figure 5C). Thus, PT-ADA-PPR exhibits two emission pathways (polythiophy

backbone and the porphyrin moiety) and could be excited by two different excitation wavelengths (488 nm and 559 nm) that match well to those commercial available fluorescence instruments used for cell imaging and bioassays.

1. Carter, K. P., Young, A. M. & Palmer, A. E. Fluorescent sensors for measuring metal ions in living systems. *Chem. Rev.* **114**, 4564–4601 (2014).
2. Nienhaus, K. & Nienhaus, G. U. Fluorescent proteins for live-cell imaging with super-resolution. *Chem. Soc. Rev.* **43**, 1088–1106 (2014).
3. Michalet, X. *et al.* Quantum dots for live cells, in vivo imaging, and diagnostics. *Science* **307**, 538–544 (2005).
4. Zeng, L., Miller, E. W., Pralle, A., Isacoff, E. Y. & Chang, C. J. A selective turn-on fluorescent sensor for imaging copper in living cells. *J. Am. Chem. Soc.* **128**, 10–11 (2006).
5. Domaille, D. W., Que, E. L. & Chang, C. J. Synthetic fluorescent sensors for studying the cell biology of metals. *Nat. Chem. Biol.* **4**, 168–175 (2008).
6. De, M. *et al.* Sensing of proteins in human serum using conjugates of nanoparticles and green fluorescent protein. *Nat. Chem.* **1**, 461–465 (2009).
7. Donner, J. S., Thompson, S. A., Kreuzer, M. P., Baffou, G. & Quidant, R. Mapping intracellular temperature using green fluorescent protein. *Nano Lett.* **12**, 2107–2111 (2012).
8. Medintz, I. L., Uyeda, H. T., Goldman, E. R. & Mattoussi, H. Quantum dot bioconjugates for imaging, labelling and sensing. *Nat. Mater.* **4**, 435–446 (2005).
9. Wang, Y., Hu, R., Lin, G., Roy, I. & Yong, K.-T. Functionalized quantum dots for biosensing and bioimaging and concerns on toxicity. *ACS Appl. Mater. Interfaces* **5**, 2786–2799 (2013).
10. Shaner, N. C. *et al.* Improving the photostability of bright monomeric orange and red fluorescent proteins. *Nat. Methods* **5**, 545–551 (2008).
11. Yang, J. *et al.* Development of aliphatic biodegradable photoluminescent polymers. *Proc. Natl. Acad. Sci. USA* **106**, 10086–10091 (2009).
12. Hardman, R. A toxicologic review of quantum dots: toxicity depends on physicochemical and environmental factors. *Environ. Healt. Perspect.* **114**, 165–172 (2006).
13. Chen, N. *et al.* The cytotoxicity of cadmium-based quantum dots. *Biomaterials* **33**, 1238–1244 (2012).
14. Stutzmann, N., Friend, R. H. & Sirringhaus, H. Self-aligned, vertical-channel, polymer field-effect transistors. *Science* **299**, 1881–1884 (2003).
15. Veres, J., Ogier, S., Lloyd, G. & de Leeuw, D. Gate insulators in organic field-effect transistors. *Chem. Mat.* **16**, 4543–4555 (2004).
16. Cheng, Y.-J., Yang, S.-H. & Hsu, C.-S. Synthesis of conjugated polymers for organic solar cell applications. *Chem. Rev.* **109**, 5868–5923 (2009).
17. Zhou, H., Yang, L. & You, W. Rational design of high performance conjugated polymers for organic solar cells. *Macromolecules* **45**, 607–632 (2012).
18. Gross, M. *et al.* Improving the performance of doped pi-conjugated polymers for use in organic light-emitting diodes. *Nature* **405**, 661–665 (2000).
19. Suh, H. *et al.* Stabilized blue emission from organic light-emitting diodes using poly(2,6-(4,4-bis(2-ethylhexyl)-4*H*-cyclopenta[*def*]phenanthrene)). *Macromolecules* **38**, 6285–6289 (2005).
20. Gaylord, B. S., Heeger, A. J. & Bazan, G. C. DNA detection using water-soluble conjugated polymers and peptide nucleic acid probes. *Proc. Natl. Acad. Sci. USA* **99**, 10954–10957 (2002).
21. Thomas III, S. W., Joly, G. D. & Swager, T. M. Chemical sensors based on amplifying fluorescent conjugated polymers. *Chem. Rev.* **107**, 1339–1386 (2007).
22. Feng, X., Liu, L., Wang, S. & Zhu, D. Water-soluble fluorescent conjugated polymers and their interactions with biomacromolecules for sensitive biosensors. *Chem. Soc. Rev.* **39**, 2411–2419 (2010).
23. Duan, X., Liu, L., Feng, F. & Wang, S. Cationic conjugated polymers for optical detection of DNA methylation, lesions, and single nucleotide polymorphisms. *Acc. Chem. Res.* **43**, 260–270 (2010).
24. McRae, R. L., Phillips, R. L., Kim, I.-B., Bunz, U. H. F. & Fahrni, C. J. Molecular recognition based on low-affinity polyvalent interactions: selective binding of a carboxylated polymer to fibronectin fibrils of live fibroblast cells. *J. Am. Chem. Soc.* **130**, 7851–7853 (2008).
25. Zhu, C., Liu, L., Yang, Q., Lv, F. & Wang, S. Water-soluble conjugated polymers for imaging, diagnosis, and therapy. *Chem. Rev.* **112**, 4687–4735 (2012).
26. Traina, C. A., Bakus II, R. C. & Bazan, G. C. Design and synthesis of monofunctionalized, water-soluble conjugated polymers for biosensing and imaging applications. *J. Am. Chem. Soc.* **133**, 12600–12607 (2011).
27. Wang, B. *et al.* Synthesis of a new conjugated polymer for cell membrane imaging by using an intracellular targeting strategy. *Polym. Chem.* **4**, 5212–5215 (2013).
28. Sista, P., Ghosh, K., Martinez, J. S. & Rocha, R. C. Polythiophenes in biological applications. *J. Nanosci. Nanotechnol.* **14**, 250–272 (2014).
29. Tang, H., Xing, C., Liu, L., Yang, Q. & Wang, S. Synthesis of amphiphilic polythiophene for cell imaging and monitoring the cellular distribution of a cisplatin anticancer drug. *Small* **7**, 1464–1470 (2011).
30. Jeffries-El, M., Sauve, G. & McCullough, R. D. Facile synthesis of end-functionalized regioregular poly(3-alkylthiophene)s via modified Grignard metathesis reaction. *Macromolecules* **38**, 10346–10352 (2005).
31. Ho, H.-A. *et al.* Colorimetric and fluorometric detection of nucleic acids using cationic polythiophene derivatives. *Angew. Chem. Int. Ed.* **41**, 1548–1551 (2002).
32. Eguilaz, M., Aguei, L., Yanez-Sedeno, P. & Pingarron, J. M. A biosensor based on cytochrome *c* immobilization on a poly-3-methylthiophene/multi-walled carbon nanotubes hybrid-modified electrode. Application to the electrochemical determination of nitrite. *J. Electroanal. Chem.* **644**, 30–35 (2010).
33. Nagarajan, S., Kumar, J., Bruno, F. F., Samuelson, L. A. & Nagarajan, R. Biocatalytically synthesized poly(3,4-ethylenedioxythiophene). *Macromolecules* **41**, 3049–3052 (2008).
34. Wang, B. *et al.* Polymer-drug conjugates for intracellar molecule-targeted photoinduced inactivation of protein and growth inhibition of cancer cells. *Sci. Rep.* **2**, 766 (2012).
35. Xing, C. *et al.* Design guidelines for conjugated polymers with light-activated anticancer activity. *Adv. Funct. Mater.* **21**, 4058–4067 (2011).
36. Wang, F. *et al.* Multi-colored fibers by self-assembly of DNA, histone proteins, and cationic conjugated polymers. *Angew. Chem. Int. Ed.* **53**, 424–428 (2014).
37. Barda, Y. *et al.* Backbone metal cyclization: novel ^{99m}Tc labeled GnRH analog as potential SPECT molecular imaging agent in cancer. *Nucl. Med. Biol.* **31**, 921–933 (2004).
38. Liu, J. *et al.* Synthesis and cancer cell cytotoxicity of gold(III) tetraarylporphyrins with a C5-carboxylate substituent. *J. Chem. Res.* **35**, 698–702 (2011).
39. Liu, K. *et al.* Supramolecular photosensitizers with enhanced antibacterial efficiency. *Angew. Chem. Int. Ed.* **52**, 8285–8289 (2013).
40. Yuan, H. *et al.* Chemical molecule-induced light-activated system for anticancer and antifungal activities. *J. Am. Chem. Soc.* **134**, 13184–13187 (2012).

Acknowledgments

This work was supported by the Major Research Plan of China (Nos. 2011CB935800, 2011CB808400) and the National Natural Science Foundation of China (Nos. 21373243, 21273254, 21021091).

Author contributions

F.W., M.L. and L.L. performed experiments, analysed data and wrote the manuscript. B.W., J.Z., Y.C. and F.L. analysed data. S.W. designed experiments, analysed data and wrote the manuscript.

Additional information

Supplementary information accompanies this paper at http://www.nature.com/scientificreports

Competing financial interests: The authors declare no competing financial interests.

How to cite this article: Wang, F. *et al.* Synthesis and Characterization of Water-Soluble Polythiophene Derivatives for Cell Imaging. *Sci. Rep.* **5**, 7617; DOI:10.1038/srep07617 (2015).

This work is licensed under a Creative Commons Attribution-NonCommercial-ShareAlike 4.0 International License. The images or other third party material in this article are included in the article's Creative Commons license, unless indicated otherwise in the credit line; if the material is not included under the Creative Commons license, users will need to obtain permission from the license holder in order to reproduce the material. To view a copy of this license, visit http://creativecommons.org/licenses/by-nc-sa/4.0/